Development of thermokinetic tools for phase transformation studies of Zr alloys in service and LOCA conditions

Caroline Toffolon-Masclet, Laure Martinelli, Clara Desgranges, Paul Lafaye, Jean-Christophe Brachet, Fabrice Legendre, Jean-Claude Crivello, Jean-Marc Joubert, Daniel Monceau

Development of thermokinetic tools for phase transformation studies of Zr alloys in service and LOCA conditions

C. Toffolon-Masclet[1], L. Martinelli[2], C. Desgranges[3], P. Lafaye[4], J.-C. Brachet[1], F. Legendre[2], J-C. Crivello[5],J-M. Joubert[5] and D. Monceau[6]

ABSTRACT

Thermodynamic and kinetic calculations are commonly used for forecasting phase transformations in multi-component alloys as a function of composition, temperature and time. They also turn to be very useful for new alloys design. Thus, in the framework of the qualification of existing industrial alloys and the development of new ones (Cr coated Zr alloys for instance), a new generation of thermodynamic database has been developed thanks to the systematic use of *ab initio* calculations. Indeed, DFT (Density Functional Theory) calculations are significant for the determination of formation enthalpies of stable and metastable phases. Moreover, SQS method (Special Quasirandom Structure) is used for the prediction of fcc, bcc and hcp mixing enthalpies in binary solid solutions.

[1] DEN-Service de Recherches Métallurgiques Appliquées, CEA, Université Paris-Saclay, F-91191Gif-sur-Yvette, France.
[2] DEN-Service de la Corrosion et du Comportement des Matériaux dans leur Environnement, CEA, Université Paris-Saclay, F-91191 Gif-sur-Yvette, France.
[3] Safran-Tech, rue des jeunes bois, Châteaufort, CS80112, 78772, Magny les hameaux, France.
[4] Centre for Research in Computational Thermochemistry (CRCT), Department of Chemical Engineering, Polytechnique Montréal, C.P. 6079, Succursale « Downtown", Montréal, Québec, H3C3A7, Canada.
[5] Université Paris Est, ICMPE (UMR 7182), CNRS, UPEC, F-94320 Thiais, France.
[6] CIRIMAT, CNRS, INPT, UPS, ENSIACET, Université de Toulouse, Toulouse Cedex 4, France.

The resulting thermodynamic database is a very powerful tool for predicting correctly Second Phase Precipitates (SPP) occurrence in industrial alloys and calculate precisely their volume fraction, chemical composition and existence domain as a function of temperature.

The second part of the paper deals with the development of the Ekinox-Zr numerical tool which has been linked to the Zr thermodynamic database using the OCASI interface of the OpenCalphad software (free software for multicomponent equilibrium calculations). This tool has been developed to simulate with accuracy oxide growth and oxygen diffusion into the alloy during high-temperature isothermal oxidation of Zr alloys. The recent developments have been dedicated to the simulation of high-temperature transients showing a good agreement with experimental data.

Keywords: Thermodynamic, kinetic, Zr-base alloys, ab-initio calculations, corrosion

Introduction

Multi-alloying and processing are important factors influencing microstructural evolutions and phase transformations in industrial Zirconium alloys. In operating or in accidental conditions in nuclear power plant, the microstructure of these alloys is modified. Thus, tools enabling the determination of phase transformation temperatures, chemical compositions and volume fractions of phases taking into account several alloying elements, are of high interest. In this context, computational thermodynamics and kinetics represent powerful tools for industrial applications. These last years, a couple of thermodynamic databases for Zr alloys have been developed using the CALPHAD modelling method [1][2]. The formalism used within the CALPHAD method enforces the description of *end-members*. In the former databases, the metastable *end-members* were given arbitrary values for the formation enthalpy, since they were not measurable

experimentally. Density Funstional Theory (DFT) calculations enabled the determination of these formation enthalpy. Thus, a new thermodynamic database for zirconium alloys has been created, including a systematic use of DFT calculations for the determination of formation enthalpies of metastable phases.

High temperature (HT) oxidation and its influence on the mechanical behavior of cladding tubes is a subject of matter as well. Indeed, during some hypothetical Pressurized Water Reactor (PWR) accidental scenario, like Loss of Coolant Accident (LOCA), the oxidation phenomena is accelerated, leading to the formation and growth of two brittle phases: ZrO_2 and α_{Zr} enriched in oxygen, from the parent β_{Zr} ductile phase. Thus, once the whole system is quenched down to room temperature, the only ductile phase is the β_{Zr} phase. It has been demonstrated that the ductility of this quenched β_{Zr} phase depends upon the O content: for oxygen contents superior to 0.4wt.%, this phase becomes brittle [3]. A tool has been developed, Ekinox-Zr [4]–[7], able to calculate the O concentration profiles in the three successive layers, ZrO_2, α_{Zr} and β_{Zr}, and the growth of these layers as a function of time at a given temperature [8]. This tool, linked to the Zircobase database and the Thermo-Calc software, has already demonstrated its ability to forecast high temperature isothermal oxidation of Zr alloys [4]–[7].

A first part of this article is dedicated to the description of the new thermodynamic database containing the following elements: Cr, Fe, Nb, Sn, Zr. Two of the 20 binary and ternary systems constituting this database, Fe-Nb and Fe-Nb-Zr, are more specifically described. Then application examples are presented illustrating the performance of the database.

The second part of this paper deals with the modification of the Ekinox-Zr code in order to simulate anisothermal oxidation transients and its linkage to the OCASI interface of the OpenCalphad software (free software for multicomponent equilibrium calculations).

Thermodynamic tool

METHODOLOGY

Calphad methodology

The Gibbs energy of each phase is described considering the sublattice model chosen and using the Compound Energy Formalism (CEF) [9].

The total molar Gibbs energy of a given α phase is expressed as follows:

$$G_m^\alpha = {}^{ref}G_m^\alpha - T\,{}^{cnf}S_m^\alpha + {}^{E}G_m^\alpha$$

where ${}^{ref}G_m^\alpha$ is the Gibbs energy surface of reference and represents the site occupancy weighted average molar Gibbs energy of the ordered structure.

${}^{cnf}S_m^\alpha$ is the configurational entropy of the α phase and is based on the number of possible arrangements of the constituents of the phase.

${}^{E}G_m^\alpha$ represents the excess Gibbs energy of mixing allowing to represent a deviation from ideality.

The crystallography of the different phases is respected, as much as possible, in the sublattice model chosen for the different phases. Furthermore, in order to give account of the existence of a homogeneity range for a given phase, all elements are allowed to enter all sublattices to reflect substitution mechanisms. Thus, the model adopted will generate so called *end-members* i.e. stoichiometric compounds corresponding to all the possible combinations with each sublattice occupied by a single element. Among them, only one corresponds to a stable phase and can be evaluated experimentally, the other ones are metastable or not stable and cannot be derived from experimental data. However, the Gibbs energies of formation of all of them appear in the expression of the total molar Gibbs energy of the phase. Thus, the formation enthalpies of the metastable or unstable phases can be calculated by *ab initio* methods.

DFT calculations

DFT calculations were performed using the Vienna Ab-Initio Simulation Package (VASP) code [10], [11]. The calculations were done using the generalized gradient approximation (GGA) with the Perdew-Burke-Ernzerhof (PBE) [12] functional and with projector augmented wave (PAW) pseudo potentials (PP).

The formation enthalpy is obtained by subtracting the total energy of the structure calculated by DFT to the molar fraction weighted sum of the energies of the pure elements in their Stable Element Reference (SER).

Mixing enthalpies were also determined for solid solutions using the SQS method [13]. It consists in generating a series of "special" configurations that reproduce the random disorder of a solid solution at a given composition with a limited number of atoms per unit cell. The quality of the "special" configuration is evaluated by comparison to its correlation function relative to those of a perfectly disordered state. The mixing enthalpy is calculated by subtracting the total energy of the SQS structure calculated by DFT to the molar fraction weighted sum of the energies of the pure elements in to the solid solution structure.

Results

THERMODYNAMIC ASSESSMENT

Among the binary and ternary systems included in the newly created thermodynamic database, the Fe-Nb-Zr ternary system and its three constitutive binary systems , Nb-Zr, Fe-Zr and Fe-Nb, will be presented hereafter.

The Nb-Zr system

The reference assessment for this system is the one of Guillermet [14]. All the available experimental and calculated data available for this system have been considered for our new assessment [15].

This new description of the Nb-Zr system is presented in FIG. *1*. It shows a slightly better agreement of the monotectoid temperature, 596°C, with experimental data, and consequently, the miscibility gap is better described.

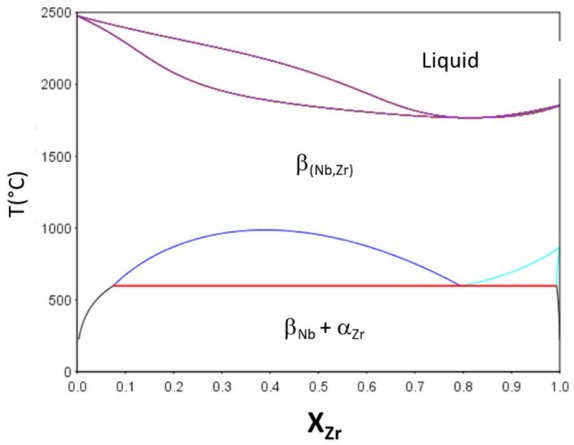

FIG. 1–Calculated Nb-Zr system calculated from [15].

The Fe-Zr binary system

The Fe-Zr system has been assessed several times using the CALPHAD method [16]–[20].

The result of our assessment is detailed in [21] and the obtained phase diagram is presented in FIG. *2*. Four intermetallic phases have been considered: two Fe_2Zr Laves phases *C*36 and *C*15, $FeZr_2$ and $FeZr_3$.

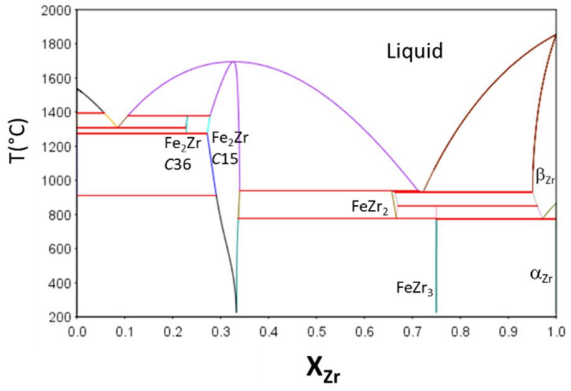

FIG. 2– Fe-Zr phase diagram calculated from [21]

This new assessment shows a very good agreement of the calculated solidus and solvus with experimental data in the Zr rich part of the system. The invariant reactions are also very well described in this part of the diagram.

The Fe-Nb binary system

Many experimental studies have been dedicated to this system [22]–[37]. Two intermetallic phases are present: Fe_2Nb (*C*14) and Fe_7Nb_6 (μ) phases.

The DFT calculations, performed at 0K, confirm the stability of the Fe_2Nb and Fe_7Nb_6 phases. Indeed the calculated ground state is in good agreement with the experimental diagram (FIG. *3*).

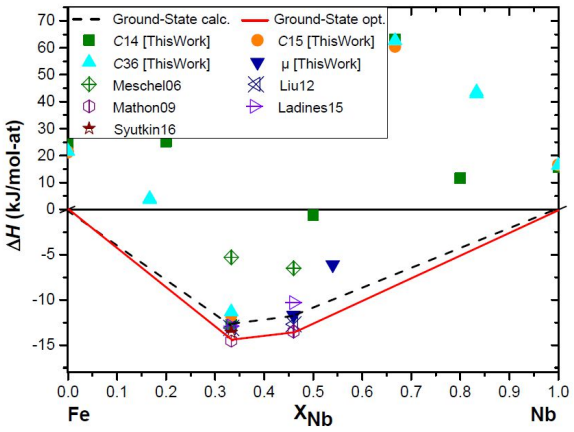

FIG. 3–Fe-Nb system: Calculated formation enthalpies of the intermetallic phases compared to experimental data (Meschel06 [38] and Syutkin06 [39]) and calculated ones (Liu12 [40], Mathon09 [41] and Ladines15 [42]).

The calculated data are in good agreement with the data from Liu et al. [40], Mathon et al. [41] and Ladines et al. [42], and the experimental one from Syutkin et al. [39] as well. The experimental data from Meschel et al. [38] show strong disagreement. The optimised ground-state is calculated from our assesment. It also shows very good agreement with the calculated one.

The calculated mixing enthalpies of the Fe solid solution (fcc) and Fe and Nb rich solid solutions (bcc) are represented in FIG. *4* and compared to optimized data from literature and from these calculations.

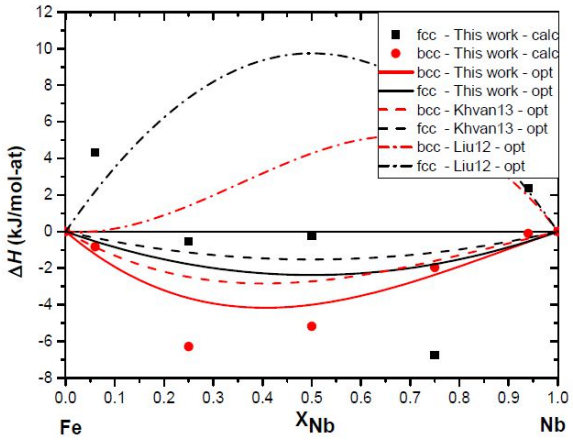

FIG. 4–Fe-Nb system : mixing enthalpies of the fcc and bcc solid solutions compared to optimised data from Khvan13 [43] and Liu12 [40]

For fcc phase, our optimized mixing enthalpy show a good agreement with the data from Khvan *et al.* [43], and a reasonable agreement with our SQS calculations. On the contrary, the data from Liu *et al*. [40] show a complete disagreement. For the bcc phase, our optimized mixing enthalpy is in good agreement with the optimized data from [43] as well. It shows attractive interaction and an assymetrical shape on the Fe rich side. Strong disagreement still exist with the data from Liu *et al.* [40].

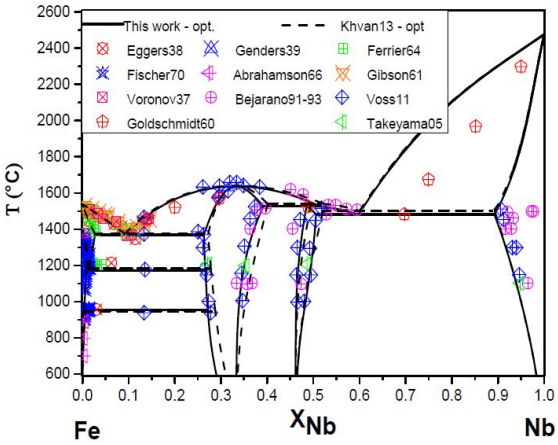

FIG. 5–Calculated Fe-Nb phase diagram compared to data from Eggers38 [23], Genders39 [30], Ferrier64 [33], Fisher70 [36], Abrahamson66 [34], Gibson61 [32], Voronov37 [22], Bejarano91-93 [24], [25], Voss11 [29]

Finally, the calculated phase diagram is presented in FIG. *5*, showing a good agreement with literature data.

The Fe-Nb-Zr ternary system

Once each binary system of interest is optimized, it is possible to start the optimization of ternary systems. Many studies have been dedicated to the Fe-Nb-Zr system [44]–[52]. Two ternary intermetallic phases are reported in this system: the hexagonal *C*14 Laves phase $(Fe,Nb)_2Zr$ and the fcc Ti_2Ni phase $(Nb,Zr)_2Fe$. A few authors [45], [53], [54] report the existence of an additional ternary phase: a hexagonal *C*36-Laves phase $Fe_2(Nb,Zr)$ (FIG. *6*).

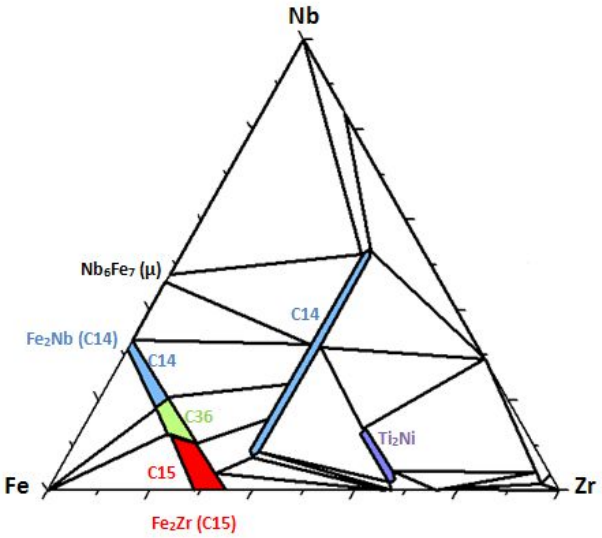

FIG. 6–Ternary isothermal section of the FeNbZr system experimentally determined at 800°C by Granovsky et al. [45]

The presence of this phase is a matter of debate. Thus, its potential existence has been checked within this work both experimentally and by DFT calculations. The experimental verification consisted in fabricating an alloy at the targeted composition, that is $Fe_2Nb_{0,5}Zr_{0,5}$. This alloy was annealed three weeks at 800°C and analyzed by X-ray diffraction and microprobe. These analyses showed the presence of two phases: Fe_2Zr (*C*15 Laves phase) and Fe_2Nb (*C*14 Laves phase).

The formation enthalpies of the *end-members* of phases Fe_2Nb (*C*14), Fe_2Zr (*C*15) and $Fe_2(Nb,Zr)$ (*C*36) have been calculated at 0K by means of DFT along the 66 at.% Fe isocomposition as represented in FIG. *7*.

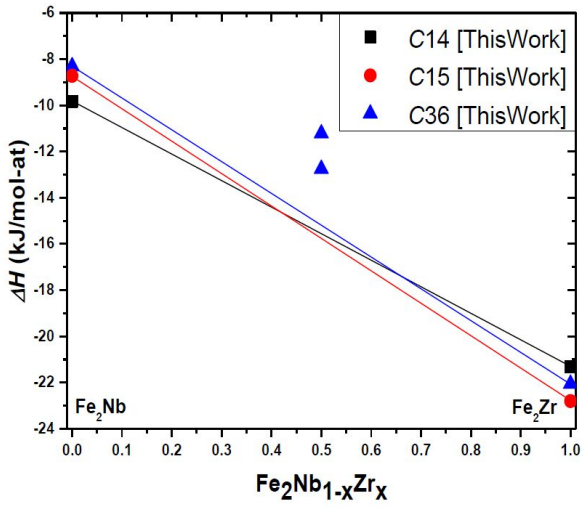

FIG. 7–Calculated formation enthalpies along the Fe_2Nb-Fe_2Zr line.

These calculations clearly show the unstability of the $Fe_2(Nb,Zr)$ (*C*36) phase along this line. The thermodynamic assessment has been done taking into account our DFT calculations and most of the experimental data. Two calculated isothermal sections are presented in FIG. *8* and. *9*. They show a good agreement with experimental data from litterature.

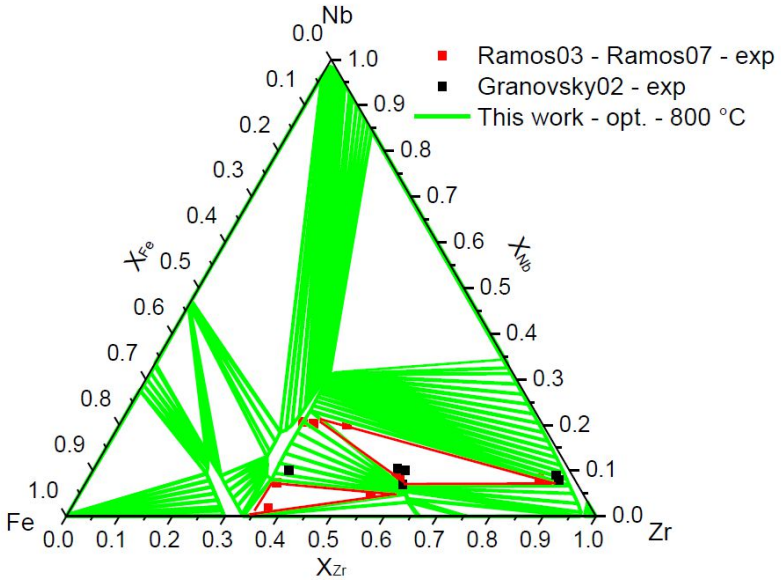

FIG. 8–Isothermal section of the Fe-Nb-Zr system calculated at 800°C and compared to experimental measurements from Ramos03-07 [46], [48] and Granovsky02 [45]

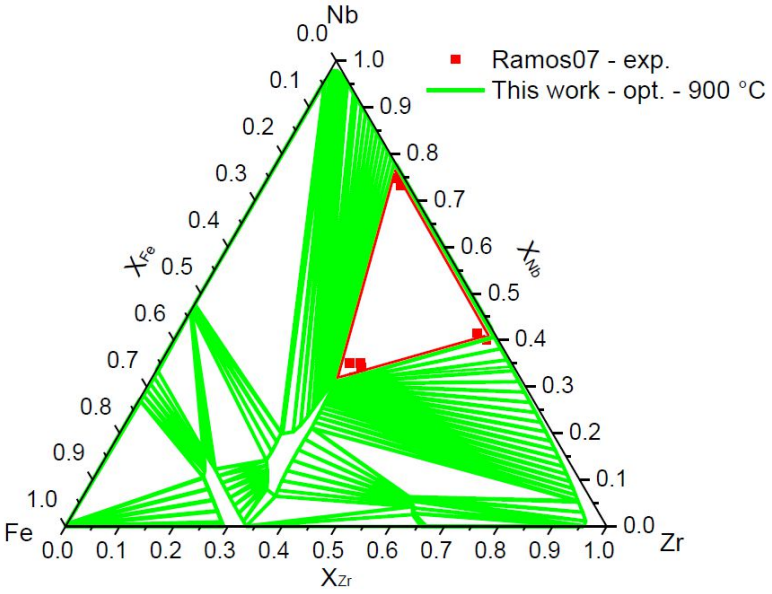

FIG. 9–Isothermal section of the Fe-Nb-Zr system calculated at 900°C and compared to experimental measurements from Ramos07 [48]

Discussion

A similar methodology has been applied to the ten binary systems and ten ternary systems constituting the quinary Zr-Cr-Fe-Nb-Sn system [15], [55] leading to a new thermodynamic database for Zr base alloys. The ten binary systems have been reassessed. Four among the ten ternary systems were completely unknown : Cr-Sn-Zr, Cr-Nb-Sn [15], Cr-Fe-Sn and Fe-Nb-Sn and have thus been studied using experiments and calculations.

The accuracy of this new database is illustrated hereafter with two different examples.

The first one comes from [52]. In this work, three ternary Fe-Nb-Zr, A1, A2 and A3 reported in TABLE 1, were fabricated and annealed at different temperatures.

TABLE 1: Nominal chemical composition of the Fe-Nb-Zr alloys from [52]

Alloy	wt.% Zr	wt.% Nb	wt.%Fe	at.%Zr	at.%Nb	at.%Fe
A1	29	51	20	26	45	29
A2	62	21	17	56	19	25
A3	73	6	21	65	5	30

The chemical composition and the volume fraction of the different phases were determined by microprobe analysis and image analysis.

FIG. *10* shows a comparison of the experimental and calculated volume fractions in the three alloys annealed at 550 and 800°C. The calculations show a good agreement with the experimental data except for alloy A2 annealed at 800°C: there is a strong discrepancy between calculations and experiments for phases $(Fe,Nb)_2Zr$ and $(Nb,Zr)_2Fe$.

A comparison between calculated and experimental chemical compositions at 550 and 800°C is shown in FIG. *11* and FIG. *12*. The agreement is satisfying except for the two solid solutions β_{Zr} and β_{Nb}.

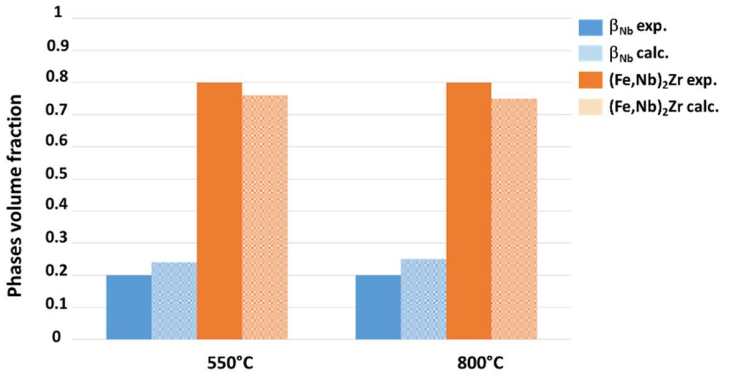

(a)

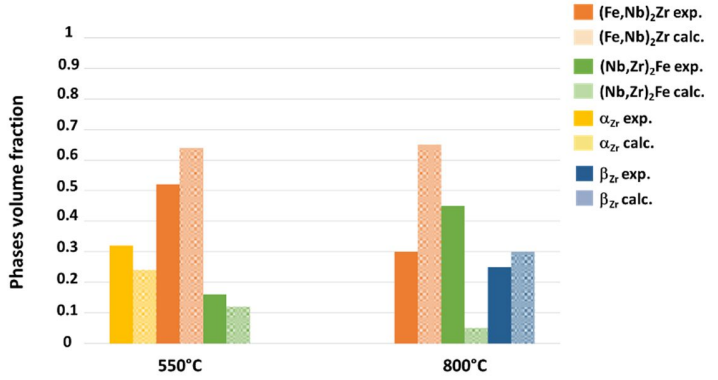

(b)

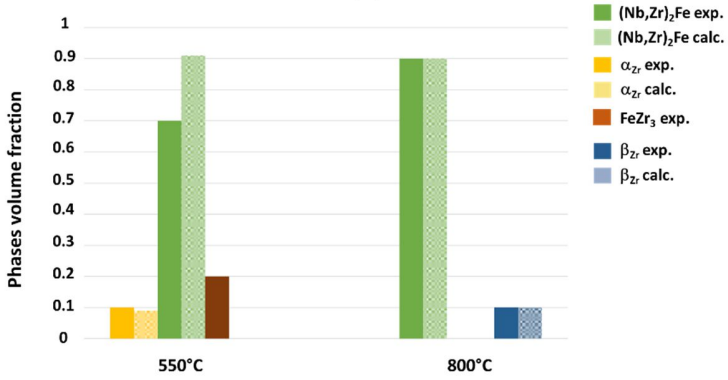

(c)

FIG. 10–Alloys A1(a), A2 (b) and A3 (c): comparison between volume fraction calculated using the new thermodynamic database and determined experimentally at 550 and 800°C.

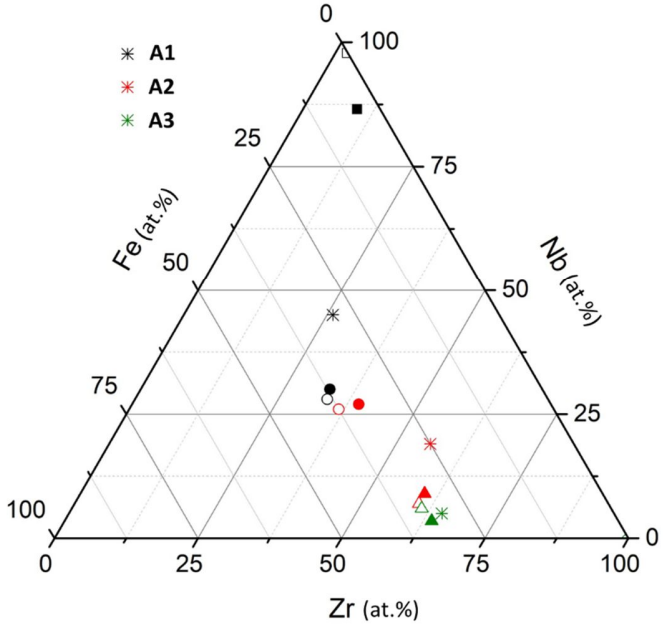

FIG. 11–Comparison between experimental and calculated phases chemical compositions in A1 (dark), A2 (red) and A3 (green) alloys at 550°C. β_{Nb} exp. filled square, β_{Nb} calc. empty square, $(Fe,Nb)_2Zr$ exp. filled circle, $(Fe,Nb)_2Zr$ calc. empty circle, $(Nb,Zr)_2Fe$ exp. filled triangle, $(Nb,Zr)_2Fe$ calc. empty triangle.

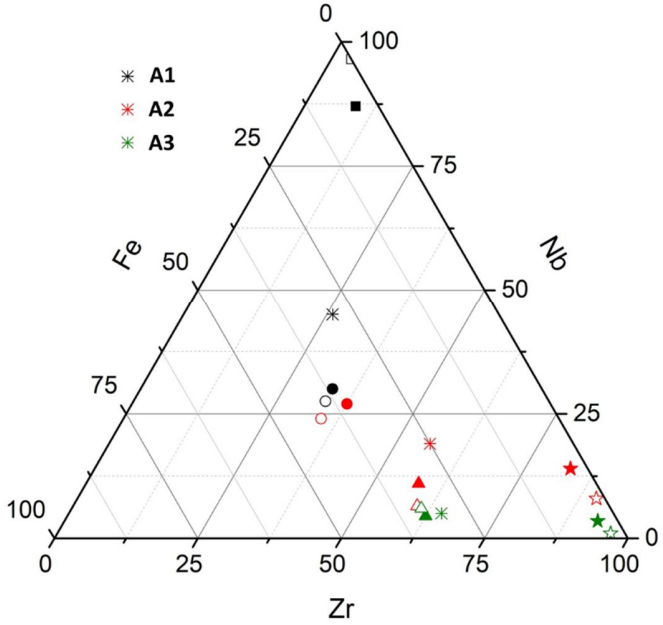

FIG. 12–Comparison between experimental and calculated phases chemical compositions in A1(dark), A2 (red) and A3 (green) alloys at 800°C. β_{Nb} exp. filled square, β_{Nb} calc. empty square, $(Fe,Nb)_2Zr$ exp. filled circle, $(Fe,Nb)_2Zr$ calc. empty circle, $(Nb,Zr)_2Fe$ exp. filled triangle, $(Nb,Zr)_2Fe$ calc. empty triangle, β_{Zr} exp. filled star, β_{Zr} calc. empty star.

The second example concerns the Zr-0.7Nb-0.3Sn-0.35Fe-0.25Cr quinary alloy that was studied experimentally by Barberis *et al*. [56]. In this work, the chemical compositions of the second phase precipitates have been measured by EDS analysis after 2h annealing treatment at 675°C. The authors report the presence of two intermetallic phases identified as Laves *C*14 phases for both of them. The thermodynamic database used in this work predicted only one intermetallic phase: the $Zr(Nb,Fe)_2$ – *C*14 phase. The calculations performed with the new thermodynamic database are reported in Table 2 and compared to the experimental measurements and predictions using the Zircobase database [1]

TABLE 2 : Comparison between predicted and measured chemical compositions of second phase precipitates in Zr-0,7Nb-0,3Sn-0,35Fe-0,25Cr annealed 2h at 675°C.

Phase	at.% Zr	at.% Nb	at.% Fe	at.% Cr	Réf.
$Zr(Nb,Fe,Cr)_2$	33,8	20,2	29,2	16,8	[56]
$Zr(Fe,Cr)_2$	33,0	4,6	29,5	32,9	[56]
$Zr(Nb,Fe)_2$ - *C*14	34,2	24,6	38,4	2,7	This work
$Zr(Fe,Cr)_2$ - *C*15	32,0	3,8	33,0	31,1	This work
$Zr(Nb,Fe)_2$ - *C*14	33,4	3,16	36,1	27,3	[1]

The Zircobase database predicts the presence of only one *C*14 $Zr(Nb,Fe)_2$ phase. The experimental measurements detected two intermetallic phases: a Nb enriched and a Nb impoverished one. The authors identified these phases as two *C*14 phases, only based on EDS measurements. Crystallographic structure determinations should be done on these samples in order to settle the right ones. Our thermodynamic calculations predict two intermetallic phases: a $Zr(Nb,Fe)_2$ - *C*14 and a $Zr(Fe,Cr)_2$ - *C*15. The calculated chemical compositions are in quite good agreement with the experimental ones.

Kinetic tool

METHODOLOGY

Ekinox-Zr

Ekinox-Zr is a numerical tool able to simulate the oxidation of zirconium alloys at high temperature [4], [5], [8]. In this model, the cladding tube is represented as a one-dimensional domain containing the successive layers: ZrO_2, $\alpha_{Zr}(O)$ and β_{Zr} . The diffusion profiles of oxygen are calculated thanks to the numerical resolution of Fick's equations with boundary conditions on moving interfaces (gas/ZrO_2, $ZrO_2/\alpha_{Zr}(O)$ and $\alpha_{Zr}(O)$ /β_{Zr}). A strong hypothesis of this code is to consider local thermodynamic equilibrium at the 3 different interfaces. Furthermore, in order to obtain accurate concentration values at the different interfaces, the code was linked to the Zircobase database via the TQ interface of Thermo-Calc.

This tool already demonstrated its ability to:

- simulate oxygen diffusion profiles in $\alpha_{Zr}(O)$ and β_{Zr} in Zr alloys during isothermal oxidation at high temperature [1100-1250°C] [8];
- take into account the influence of hydrogen of HT oxidation [5]
- take into account the effect of a pre-oxide layer presence on the oxygen concentration profile during HT oxidation [6]

The new development of the Ekinox-Zr code presented hereafter concerned the simulation of anisothermal transients.

Results and discussion

The Ekinox-Zr code has been recently linked to the Zircobase via the OCASI interface of the OpenCalphad software. OpenCalphad is a free software for multicomponent equilibrium calculations similar to Thermo-Calc. Then, the code has been modified in order to be able to calculate anisothermal transients. Anisothermal calculations have been performed and compared to experimental data obtained on Zy-4 alloy.

The experimental oxidations were performed under a mixture containing 60% O_2 / 40% He using Thermogravimetric analysis.

The experimental oxidation kinetics obtained for two different heating rates, 2 and 20°C/min between 1100 and 1275°C, are compared to Ekinox-Zr simulations in Figure 13.

For both heating rates, 2 and 20°C/min, the experimental kinetics deviate from the usual parabolic kinetics (Figure 13b and d) after respectively 1300 s and 165 s of oxidation. These oxidation durations correspond to roughly 1144°C and 1155°C respectively. This breakaway oxidation is not reproduced by simulation. It is attributed to the occurrence of the ZrO_2 monoclinic to ZrO_2 tetragonal phase transformation that leads to micro-cracking of the oxide scale and consequently to the breakaway oxidation. This refinement is not included yet in the Ekinox-Zr code: only a global ZrO_2 layer is taken into account. Different studies tend to demonstrate that the tetragonal structure of zirconia is stabilized at temperatures inferior to its existence temperature range, at the metal / oxide interface thanks to the existence of stresses [57]–[61]. Thus, Ekinox-Zr could be modified to take into account two different layers in the zirconia phase. This is one of the development perspective of the code.

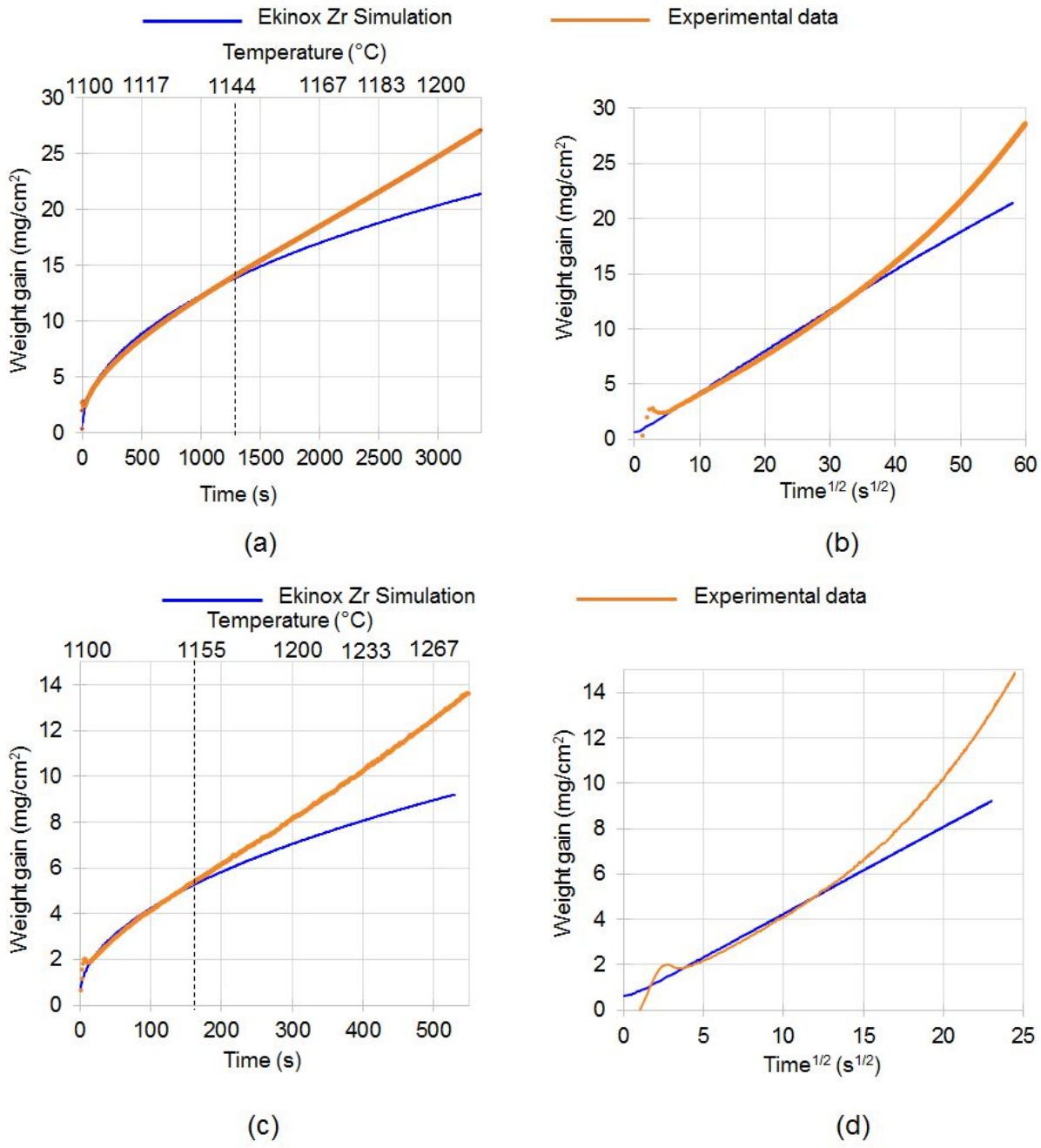

FIG. 13–Anisothermal oxidations of Zy-4 alloy at 2°C/min (a) and 20°C/min (c) between 1100 and 1275°C. (b) and (d) represent the corresponding weight gain as a function of the square root of time.

However, before the breakaway, the Ekinox-Zr code reproduces very well the parabolic oxidation kinetics. This agreement between experiments and calculation shows that the code is now able to forecast oxidation kinetics in anisothermal conditions before the breakaway occurrence. One of

the interest of the Ekinox-Zr code is to calculate oxygen concentration profiles in the metallic phases involved in the oxidation process. Such oxygen concentration profiles are represented in Figure 14 for both heating rates (2 and 20°C/min) and two conditions: at T=1133°C (Figure 14a) and after 200 s (Figure 14b) of anisothermal oxidation. The calculated profiles are consistent: at a given temperature, the cladding submitted to the slower heating rate is more oxidized as the thickness of the α_{Zr} phase is higher for the alloy heated at 2°C/min compared to the one heated at 20°C/min. The volume fraction of brittle phase is thus superior. However, for an equivalent low time of oxidation (200 s), the concentration profiles are quite similar. The oxygen uptake is similar but slightly higher in the α_{Zr} phase for the 2°C/min ramp and slightly higher in the β_{Zr} phase for the 20°C/min ramp. This result can be explained by the oxygen concentrations at the α_{Zr}/β_{Zr} interface that are higher in both phases for the 20°C/min ramp: the higher oxygen concentration in the α_{Zr} phase reduces the α_{Zr} phase growth, and the higher O flux within the β_{Zr} phase induces a higher O flux within the β_{Zr} layer.

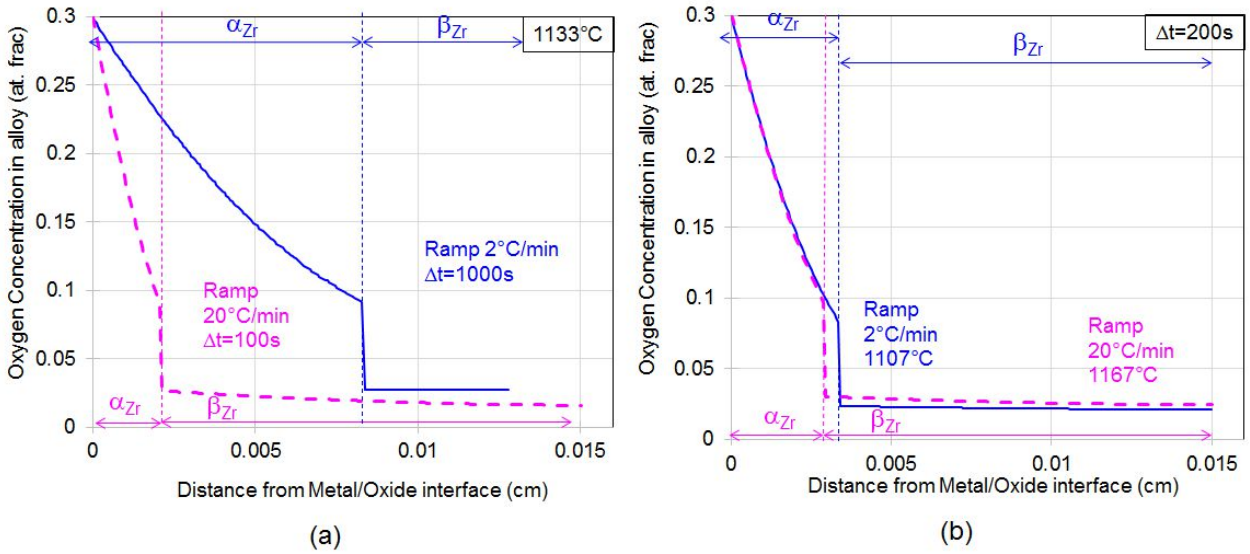

FIG. 14–Calculated concentration profiles in Zy-4 alloy for anisothermal oxidation at two different heating rates: 2 and 20°C/min and for two different conditions: at T=1133°C (a) and after 200 s of oxidation (b).

Conclusions

This study highlights many advances both in Zr alloys thermodynamics and in Zr alloys oxidation kinetics:

- a new thermodynamic database for zirconium alloys, containing the Cr-Fe-Nb-Sn-Zr elements, has been developed, implying the systematic use of DFT calculation for the determination of specific parameters for formation enthalpies of metastable phases.
- The ten binary and ten ternary systems constituting this database have been reassessed implying experimental verification for some of them. Hence, the non-stability of the *C*36-Laves in the Fe-Nb-Zr system has been demonstrated.
- The use of this database for thermodynamic computations show very good agreement with experimental data. These agreements demonstrate the consistency of the new thermodynamic database.
- The Ekinox-Zr numerical code enabling the calculation of oxidation kinetics and oxygen concentration profiles in Zr alloys during high temperature oxidation has been improved to allow anisothermal calculations.

References

[1] N. Dupin, I. Ansara, C. Servant, C. Toffolon, C. Lemaignan, and J.-C. Brachet, "Thermodynamic database for zirconium alloys," *J. Nucl. Mater.*, vol. 275, no. 3, pp. 287–295, 1999.

[2] P. Barberis *et al.*, "Microstructure and phase control in Zr-Fe-Cr-Ni alloys: Thermodynamic and kinetic aspects," in *ASTM Special Technical Publication*, 2005, no. 1467.

[3] J.-C. Brachet *et al.*, "Hydrogen content, Preoxidation, and Cooling Scenario Effects on Post-Quench Microstructure and Mechanical Properties of Zircaloy-4 and M5 Alloys in LOCA Conditions," *J. ASTM Int.*, vol. 5, no. 5, 2008.

[4] C. Toffolon-Masclet, C. Desgranges, C. Corvalan-Moya, and J.-C. Brachet, "Simulation of the β→α(O) Phase Transformation due to Oxygen Diffusion during High Temperature

Oxidation of Zirconium Alloys," *Solid State Phenom.*, vol. 172–174, pp. 652–657, 2011.
[5] B. Mazères, C. Desgranges, C. Toffolon-Masclet, and D. Monceau, "Contribution to modeling of hydrogen effect on oxygen diffusion in Zy-4 alloy during high temperature steam oxidation," *Oxid. Met.*, vol. 79, no. 1–2, 2013.
[6] B. Mazères, C. Desgranges, C. Toffolon-Masclet, and D. Monceau, "Experimental study and numerical simulation of high temperature (1100–1250 °C) oxidation of prior-oxidized zirconium alloy," *Corros. Sci.*, vol. 103, pp. 10–19, Feb. 2016.
[7] B. Mazères, C. Desgranges, C. Toffolon-Masclet, and D. Monceau, "Modeling Two- and Three-Stage Oxygen Tracer Experiments during High-Temperature Oxidation of Metals with a High Oxygen Solubility," *Oxid. Met.*, 2017.
[8] C. Corvalan-Moya, C. Desgranges, C. Toffolon-Masclet, C. Servant, and J.-C. Brachet, "Numerical modeling of oxygen diffusion in the wall thickness of Low-Tin Zircaloy-4 fuel cladding tube during high temperature (1100-1250 °C) steam oxidation," *J. Nucl. Mater.*, vol. 400, no. 3, pp. 196–204, May 2010.
[9] M. Hillert, "The compound energy formalism," *J. Alloys Compd.*, vol. 320, no. 2, pp. 161–176, 2001.
[10] G. Kresse and J. Furthmüller, "Efficient iterative schemes for ab initio total-energy calculations using a plane-wave basis set," *Phys. Rev. B - Condens. Matter Mater. Phys.*, vol. 54, no. 16, pp. 11169–11186, 1996.
[11] G. Kresse and D. Joubert, "From ultrasoft pseudopotentials to the projector augmented-wave method," *Phys. Rev. B - Condens. Matter Mater. Phys.*, vol. 59, no. 3, pp. 1758–1775, 1999.
[12] J. P. Perdew, K. Burke, and M. Ernzerhof, "Generalized gradient approximation made simple," *Phys. Rev. Lett.*, vol. 77, pp. 3865–3868, 1996.
[13] A. Zunger, S.-H. Wei, L. G. Ferreira, and J. E. Bernard, "Special Quasi Random Structures," *Phys. Rev. Lett.*, vol. 65, no. 3, pp. 353–356, 1990.
[14] A. Guillermet, "Thermodynamic Analysis of the Stable Phases in the Zr-Nb System and Calculation of the Phase-Diagram," *Z. Met.*, vol. 82, pp. 478–487, 1991.
[15] P. Lafaye, C. Toffolon-Masclet, J.-C. Crivello, and J.-M. Joubert, "Experimental investigations and thermodynamic modelling of the Cr-Nb-Sn-Zr system," *Calphad Comput. Coupling Phase Diagrams Thermochem.*, vol. 64, pp. 43–54, 2019.
[16] C. Servant, C. Guéneau, and I. Ansara, "Experimental and thermodynamic assessment of the Fe-Zr system," *J. Alloy. Compd.*, vol. 220, pp. 19–26, 1995.
[17] M. Jiang, K. Oikawa, T. Ikeshoji, L. Wulff, and K. Ishida, "Thermodynamic calculations of Fe-Zr and Fe-Zr-C systems," *J. Phase Equilibria*, vol. 22, pp. 406–417, 2001.
[18] V. Rigaud, B. Sundman, D. Daloz, and G. Lesoult, "Thermodynamic assessment of the Fe-Al-Zr phase diagram," *Calphad Comput. Coupling Phase Diagrams Thermochem.*, vol. 33, pp. 442–449, 2009.
[19] C. Guo, Z. Du, C. Li, B. Zhang, and M. Tao, "Thermodynamic description of the Al-Fe-Zr system," *Calphad Comput. Coupling Phase Diagrams Thermochem.*, vol. 32, pp. 637–649, 2008.
[20] Y. Yang, L. Tan, H. Bei, and J. T. Busby, "Thermodynamic modeling and experimental study of the Fe-Cr-Zr system," *J. Nucl. Mater.*, vol. 441, pp. 190–202, 2013.
[21] P. Lafaye, C. Toffolon-Masclet, J.-C. Crivello, and J.-M. Joubert, "New experimental study, first-principles calculations and thermodynamic modelling of the ternary Fe-Sn-Zr system," *Intermet. to be Publ.*

[22] N. M. Voronov, “N,” *Izv Akad Nauk SSSR Khim*, vol. 1, pp. 1369–1379, 1937.
[23] H. Eggers and W. Peter, “No,” *Mitt Kaiser-Wilhelm Inf Eisenforsch.*, vol. 20, pp. 199–203, 1938.
[24] J. Bejarano, S. Gama, C. Ribeiro, G. Effenberg, and C. Santos, “On the existence of the Fe2Nb3 phase in the Fe-Nb system,” *Z. Met.*, vol. 82, no. 8, pp. 615–620, 1991.
[25] J. Bejarano, S. Gama, C. Ribeiro, and G. Effenberg, “the iron-niobium phase,” *Z. Met.*, vol. 84, no. 3, pp. 160–164, 1993.
[26] C. G. Schon, J. Albert, and S. Ten, “The chemistry of the iron-niobium intermetallics,” vol. 9795, no. 95, pp. 211–216, 1996.
[27] M. Takeyama, N. Gomi, S. Morita, and T.Matsuo, “Phase equilibria and lattice parameters of Fe2Nb laves phase in Fe-Ni-Nb ternarysystem at elevated temperatures,” in *Integr. Interdiscip. Asp. Intermet*, 2005, pp. 461–466.
[28] S. K. Balam and A. Paul, “Interdiffusion study in the Fe-Nb system,” *Metall. Mater. Trans. A - Phys. Metall. Mater. Sci.*, vol. 41, no. September, pp. 2175–2179, 2010.
[29] S. Voss, M. Palm, F. Stein, and D. Raabe, “Phase Equilibria in the Fe-Nb System,” *J. Phase Equilibria Diffus.*, vol. 32, no. 2, pp. 97–104, 2011.
[30] R. Genders and R. Harrison, “N,” *J. Iron Steel Inst.*, vol. 140, pp. 29–37, 1939.
[31] H.J. Goldschmidt, “No,” *J. Iron Steel Inst.*, vol. 194, pp. 169–180, 1960.
[32] W. S. Gibson, J. R. Lee, and W. Hume-Rothery, “N,” *J. Iron Steel Inst.*, vol. 198, pp. 64–66, 1961.
[33] A. Ferrier, E. Wachtel, and E. Ubelacker, “Etude du diagramme Fer-Niobium entre 0 et 12 at % de niobium dans l’intervalle 1200-1535 °C,” *Comptes Rendus hebd. séances Acad. Sci.*, vol. 258, p. 5424, 1964.
[34] E. P. Abrahamson and S. L. Lopata, “The lattice parameters and solubility limits of alpha iron as affected by some binary transition-element additions,” *Trans. Met. Soc. AIME.*, vol. 236, pp. 76–87, 1966.
[35] P. Kripyakevich, E. I. Gladyshe, and R. V. Skolozdr, “W6Fe7-Type compounds in Nb-Fe, Ta-Fe and Ta-Co systems,” *Sov. Phys. Crystallogr*, vol. 12, p. 525, 1968.
[36] W. Fischer, K. Lorenz, H. Fabritius, and D. Schlegel, “Examination of a gamma transformation in very pure binary alloys of iron with molybdenum, vanadium, tungsten, niobium, tantalum, zirconium and cobalt,” *Arch. Eisenhuttenwes.*, vol. 41, p. 489, 1970.
[37] M. Drys, J. Sosnowski, and L. Folcik, “Phase equilibira in the niobium-gallium-iron system at 1000°C,” *J. Less-Common Met.*, vol. 68, pp. 175–181, 1979.
[38] S. V. Meschel and O. J. Kleppa, “Standard enthalpies of formation of some 3d, 4d and 5d transition-metal stannides by direct synthesis calorimetry,” *Thermochim. Acta*, vol. 314, pp. 205–212, 1998.
[39] E. A. Syutkin, A. Jacob, C. Schmetterer, A. V Khvan, B. Hallstedt, and A. T. Dinsdale, “Thermochimica Acta Experimental determination of the thermodynamic properties of the Laves phases in the Cr – Fe – Nb system,” *Thermochim. Acta*, vol. 624, pp. 47–54, 2016.
[40] S. Liu, B. Hallstedt, D. Music, and Y. Du, “CALPHAD : Computer Coupling of Phase Diagrams and Thermochemistry Ab initio calculations and thermodynamic modeling for the Fe – Mn – Nb system,” *Calphad*, vol. 38, pp. 43–58, 2012.
[41] M. Mathon, D. Connétable, B. Sundman, and J. Lacaze, “CALPHAD : Computer Coupling of Phase Diagrams and Thermochemistry Calphad-type assessment of the Fe – Nb – Ni ternary system,” *Calphad Comput. Coupling Phase Diagrams Thermochem. \futurelet \@let@token Thermochem.*, vol. 33, no. 1, pp. 136–161, 2009.

[42] A. N. Ladines, T. Hammerschmidt, and R. Drautz, “Intermetallics Structural stability of Fe-based topologically close-packed phases,” *Intermetallics*, vol. 59, pp. 59–67, 2015.
[43] A. V Khvan and B. Hallstedt, “CALPHAD : Computer Coupling of Phase Diagrams and Thermochemistry Thermodynamic description of the Fe – Mn – Nb – C system,” *Calphad*, vol. 39, pp. 62–69, 2012.
[44] C. Ramos, C. Saragovi, M. S. Granovsky, and D. Arias, “Mossbaueur spectroscopy of the Zr-rich region in Zr-Nb-Fe alloys with low Nb content,” *Hyperfine Interact.*, vol. 122, pp. 201–207, 1999.
[45] M. S. Granovsky, M. Canay, E. Lena, and D. Arias, “Experimental Investigation of the Zr corner of the Ternary Zr-Nb-Fe Phase Diagram,” *J. Nucl. Mater.*, vol. 302, pp. 1–8, 2002.
[46] C. Ramos, C. Saragovi, M. S. Granovsky, and D. Arias, “Effects of Nb content on the Zr2Fe Intermetallic stability,” *J. Nucl. Mater.*, vol. 312, pp. 266–269, 2003.
[47] H.-G. Kim, J.-Y. Park, and Y.-H. Jeong, “Ex-reactor corrosion and oxide characteristics of Zr-Nb-Fe alloys with the Nb/Fe ratio,” *J. Nucl. Mater.*, vol. 345, pp. 1–10, 2005.
[48] C. Ramos, C. Saragovi, and M. S. Granovsky, “Some new experimental results on the Zr-Nb-Fe system,” *J. Nucl. Mater.*, vol. 366, pp. 198–205, 2007.
[49] C. P. Ramos, M. S. Granovsky, and C. Saragovi, “Mossbauer spectrocopy characterization of Zr-Nb-Fe phases,” *Phys. Condens. Matter.*, vol. 389, pp. 67–72, 2007.
[50] Z. M. Alekseeva and N. V. Korotkova, “Isotermitcheskie cetchnia diagrammi sostoiania Zr-Nb-Fe v’intervale temperatour 1600-850°C,” *Izv. Akad. Nauk. SSSR, Met.*, vol. 4, no. 1, pp. 199–205, 1989.
[51] N. V. Korotkova and Z. M. Alekseyeva, “Topologia diagrammi sostaiania Zr-Nb-Fe v’intervale temperatour 500-800°C,” *Izv. Akad. Nauk. SSSR, Met.*, vol. 5, no. 3, pp. 207–214, 1989.
[52] C. Toffolon-Masclet *et al.*, “Contribution of Thermodynamic Calculations to Metallurgical Studies of Multi-Component Zirconium Based Alloys,” *J. ASTM Int.*, vol. 5, no. 7, pp. 754–775, 2008.
[53] J. Liang *et al.*, “Contribution on the phase equilibria in Zr-Nb-Fe system,” *J. Nucl. Mater.*, vol. 466, pp. 627–633, 2015.
[54] C. Arreguez, M. R. Tolosa, D. Arias, C. Corvalan, and N. Nieva, “Short communication on experimental phase diagram of the Fe corner in the Fe-Nb-Zr system at 800 C,” vol. 509, pp. 158–161, 2018.
[55] P. Lafaye, C. Toffolon-Masclet, J.-C. Crivello, and J.-M. Joubert, “Thermodynamic modelling of the Cr-Nb-Sn system,” *Calphad Comput. Coupling Phase Diagrams Thermochem.*, vol. 57, 2017.
[56] P. Barberis, C. Vauglin, P. Fremiot, and P. Guerin, “Thermodynamics of Zr Alloys: Application to Heterogeneous Materials,” in *Zirconium in the Nuclear Industry: 17th International symposium. STP 1543*, 2015, pp. 118–137.
[57] R. C. Garvie, “Stabilization of the tetragonal structureof zirconia microcrystals,” *J. Phys. Chem.*, vol. 82, pp. 218–224, 1978.
[58] G. Baldinozzi, D. Simeone, D. Gosset, and M. Dutheil, “Neutron diffraction study of the size-induced tetragonal to monoclinic phase transition in zirconia nanocrystals,” *Phys. Rev. Lett.*, vol. 90, pp. 216103-1–4, 2003.
[59] I. Kasatkin *et al.*, “HRTEM observation of the monoclinic-to-tetragonal (m-t) phase transition in nanocrystallite ZrO2,” *J. Nucl. Sci.*, vol. 39, pp. 2151–2157, 2004.
[60] R. C. Garvie and M. V. Swain, “Thermodynamics of the tetragonal to monoclinic phase

transformation in constrained zirconia microcrystals - Part. I In the absence of an applied stress field," *J. Mater. Sci.*, vol. 20, pp. 1193–1200, 1985.
[61] R. C. Garvie, "Thermodynamics of the tetragonal to monoclinic phase transformation in constrained zirconia microcrystals - Part. 2 In the presence of an applied stress field," *J. Mater. Sci.*, vol. 20, pp. 3479–3486, 1985.